

# On the effectiveness of Rotation-Equivariance in U-Net: A Benchmark for Image Segmentation

Anonymous authors

Paper under double-blind review

## Abstract

Numerous studies have recently focused on incorporating different variations of equivariance in Convolutional Neural Networks (CNNs). In particular, rotation-equivariance has gathered significant attention due to its relevance in many applications related to medical imaging, microscopic imaging, satellite imaging, industrial tasks, etc. While prior research has primarily focused on enhancing classification tasks with rotation equivariant CNNs, their impact on more complex architectures, such as U-Net for image segmentation, remains scarcely explored. Indeed, previous work interested in integrating rotation-equivariance into U-Net architecture have focused on solving specific applications with a limited scope. In contrast, this paper aims to provide a more exhaustive evaluation of rotation equivariant U-Net for image segmentation across a broader range of tasks. We benchmark their effectiveness against standard U-Net architectures, assessing improvements in terms of performance and sustainability (i.e., computational cost). Our evaluation focuses on datasets whose orientation of objects of interest is arbitrary in the image (e.g., Kvasir-SEG), but also on more standard segmentation datasets (such as COCO-Stuff) as to explore the wider applicability of rotation equivariance beyond tasks undoubtedly concerned by rotation equivariance. The main contribution of this work is to provide insights into the trade-offs and advantages of integrating rotation equivariance for segmentation tasks.

## 1 Introduction

Recently, many studies have focused on integrating different forms of equivariance in Convolutional Neural Networks (CNNs) (Weiler & Cesa, 2019; Delchevalerie et al., 2023; Worrall et al., 2017; Cohen & Welling, 2016; Kumar et al., 2018). This idea is largely inspired from the superior ability of CNNs to solve image-related tasks (e.g., classification, detection, segmentation) compared to fully-connected architectures. Indeed, CNNs inherently leverage translation equivariance (i.e., shifts in position) equivariance by extracting features through the use of convolutions that implement weight sharing across translations. This property is particularly desirable for solving image processing tasks. This sharing of weights leads to models that are more efficient in image processing, both in term of accuracy and computational resources as compared to their fully-connected counterparts.

In previous work on introducing equivariance in CNNs, rotation equivariance has attracted particular attention. As a matter of fact, rotation equivariance is highly relevant for many applications, especially when the overall orientation of the image is arbitrary. Such cases arise in many fields, including medical imaging (Or-eiller et al., 2022; Elaldi et al., 2024), microscopic imaging Chidester et al. (2019b); Graham et al. (2020), satellite imaging Marcos et al. (2018); Li et al. (2020) and industry 4.0 (Marcos et al., 2016). In those cases, the overall orientation of the images often contains no meaningful information. Instead, this orientation adds noise, potentially hindering the training process of a model. As a result, constraining CNNs with rotation equivariance can incorporate prior knowledge into the model, thereby improving its performance thanks to a reduction in unnecessary variability.

When applied to relevant tasks, rotation equivariant CNNs can outperform their vanilla counterparts (Weiler & Cesa, 2019; Worrall et al., 2017; Delchevalerie et al., 2023). Specifically, equivariant CNNs often achieve

higher accuracy or at least state-of-the-art performances while using fewer parameters. This leads to an improvement from a sustainability point of view, since training models with fewer parameters reduce the overall computational cost. However, only a few studies have evaluated the benefit of these techniques in more complex CNN architectures or on tasks beyond classification (Chidester et al., 2019a; Mitton & Murray-Smith, 2021; Oreiller et al., 2022). Furthermore, while it is well-established that rotation equivariance is beneficial for specific applications that involve arbitrary orientations, it may also prove to be useful for more general tasks that do not inherently require global rotation invariance *a priori*. In fact, learning rotation equivariant features can still help in solving such tasks more effectively.

In this work, we explore the impact of rotation equivariance on segmentation tasks, in particular, using the popular U-Net (Ronneberger et al., 2015) architecture. While most prior research has focused on evaluating the benefits of equivariant CNNs for classification tasks, we aim to fill the gap by benchmarking their performance on the more complex task of image segmentation. We assess whether introducing rotation equivariance can improve model accuracy, reduce the computational resources required by the model, or even both. Moreover, we also evaluate equivariant models for tasks where the orientation of the image is not necessarily arbitrary or not explicitly related to the task, such as objects segmentation (e.g., building or ship) in aerial imagery, where these maintain consistent orientations relative to the ground. For example, recognizing buildings or ships in aerial images. This is mainly motivated by the fact that learning rotation invariant features can still be useful for such applications, where the performance of equivariant model is higher. This justifies the use of standard segmentation datasets that focus on general tasks (such as the well-known COCO-Stuff (Lin et al., 2014)) along with others datasets that are more linked to the concept of rotation invariance and focus on specific, narrow tasks (e.g., Kvasir-SEG (Jha et al., 2020), a dataset for polyp detection in colonoscopy images). In this work, we provide a comprehensive analysis of the trade-offs and advantages of incorporating rotation equivariance into U-Net, thereby contributing to a broader understanding of its applicability across a range of use cases. The PyTorch implementation of our work will be open sourced upon final acceptance of our paper.

Section 2 provides a background knowledge on equivariance in CNNs, as well as on the U-Net architecture. Subsequently, Section 3 presents the related work on using equivariant models for segmentation tasks. Then, the datasets and models considered in assessing the usefulness of equivariant U-Nets are presented in Section 4, while the experiments and results are presented in Section 5. Finally, Section 6 presents a discussion on the results before concluding in Section 7.

## 2 Background

This section provides background knowledge about the task of image segmentation and the U-Net architecture. Furthermore, it presents the current state-of-the-art techniques that allow for the implementation of equivariance in CNNs.

### 2.1 U-Net

Segmentation models are a critical class of deep learning architectures designed for pixel-wise classification tasks, where the goal is to assign a label to each pixel in an image. This is essential in various domains such as medical imaging, autonomous driving, and satellite imagery, where understanding the spatial structure of objects within an image is necessary for predicting segmentation masks. Among these models, U-Net (Ronneberger et al., 2015) has emerged as one of the most popular and effective architectures for image segmentation. This model was originally developed for biomedical image segmentation and has since been widely adopted across different fields. The model has a 'U' shape and is based on an encoder-decoder structure with skip connections (see Figure 1), where the encoder is responsible for extracting hierarchical features and the decoder focuses on reconstructing segmentation masks. The ability of U-Net to combine low-level spatial details with high-level semantic information makes it particularly effective for boundary delineation at the pixel-level. This end-to-end architecture is capable of producing segmentation masks for objects of arbitrary shapes, distinguishing it from other contemporary architectures such as YOLO (Redmon et al., 2016), which are typically limited to generating bounding boxes.

The encoder aims at progressively extracting useful information at different scales in the input image. It is responsible for capturing the context of the input image through a series of downsampling convolutional layers. Each layer in the encoder path applies a set of convolutional operations followed by activation functions and pooling operations. This process progressively reduces the spatial dimensions of the input, while increasing the number of feature channels, effectively condensing the image information into a much more compact representation. At the bottom of the U-shape (after the encoder), one finds the bottleneck layer. It acts as the bridge between the encoder and decoder, and consists of convolutional operations that further distill the compact representation of the image. This allows the network to capture complex and abstract patterns within the input data. Afterwards, the aim of the decoder is to reconstruct an output image with the initial spatial dimensions. It employs transposed convolutions (also known as up-convolutions) to upsample the feature maps, gradually restoring the spatial dimensions that were reduced during the encoding process. A core feature of the U-Net architecture is its skip connections between the encoder and decoder layers. When the input data moves downward the encoder (e.g., a  $224 \times 224$  pixels image), it undergoes successive downsampling operations that increase the receptive field and capture abstract features. Unfortunately, the corollary is that fine spatial details are lost. Nonetheless, the skip connections address this limitation by connecting each encoder layer to its corresponding decoder layer (i.e., there is a one-to-one mapping between each encoder and each decoder layer) in order to concatenate their feature maps. This allows high-resolution spatial information to flow from the early encoder layers (at the top of the U-Net) to the decoder. Moreover, the abstract features learned at the bottom of the U-Net (i.e., in the bottleneck) are preserved. In medical image segmentation for instance, these connections help preserve boundary details and anatomical structures that might otherwise be lost during the encoding process.

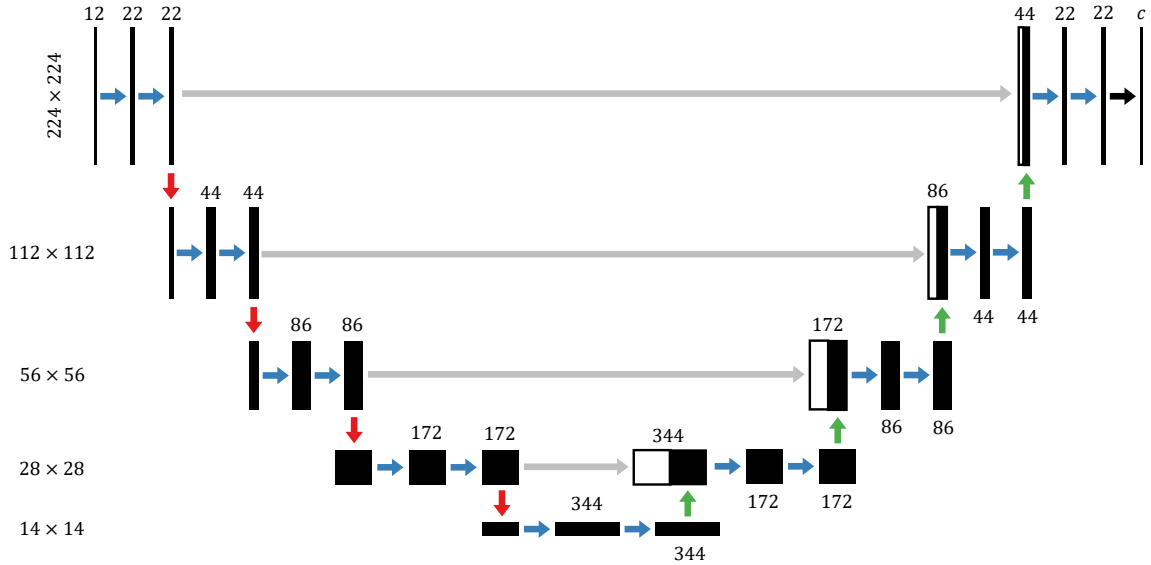


Figure 1: The U-Net architecture for the large vanilla U-Net (adapted from Ronneberger et al. (2015)). It illustrates the encoder, bottleneck, and decoder paths with skip connections. Input image is preprocessed by two convolutional layers (not represented in this illustration). Red arrows correspond to downsampling, blue arrows to convolutions and green arrows to upsampling. The final image obtained after the last black arrow are the  $c$  segmentation masks for the  $c$  corresponding classes.

The U-Net architecture is particularly effective in scenarios with limited training data, which is common in medical imaging and other specialized fields. The extensive use of data augmentation, along with the skip connections that help preserve spatial information, allows U-Net to produce precise segmentation maps even when trained on small datasets. Furthermore, its ability to work end-to-end makes it a preferred choice for segmentation tasks that require detailed, pixel-level accuracy.

## 2.2 Equivariance in CNNs

Recently, numerous studies have focused on incorporating equivariance in CNNs. Rotation equivariance, in particular, has attracted significant attention due to its relevance in image recognition. The property of rotation equivariance is very important in several domains, like medical, satellite, and microscopy imaging where the orientation of objects can be arbitrary, meaning that any variation in the orientation of the object should not affect their classification or detection (Weiler & Cesa, 2019). This means that some images do not have a preferred global orientation. For example, it is the case for a building in satellite imagery, where regardless of the viewing angle from above (i.e., aerial view), it is still the same object. Medical scans are another concrete examples, where a tumor should be recognizable regardless of the patient’s position in the machine during the capture of the images.

There are three categories of methods that deal with rotation equivariance: (i) those that enhance rotation robustness without providing formal guarantees of equivariance, (ii) those that offer some mathematical guarantees, but only for a discrete set of rotations, such as those defined by the cyclic  $C_n$  and dihedral  $D_n$  groups, and (iii) those that give mathematical guarantees of equivariance for continuous transformations, primarily involving the special orthogonal  $SO(2)$  or the orthogonal  $O(2)$  groups.

The most famous technique from the first category is data augmentation (Quiroga et al., 2018). The main idea of data augmentation is to artificially increase the size of the training set by incorporating variability in the data that is unrelated to the considered task. In the context of rotation equivariance, one may introduce rotated versions of the images in the training dataset, for example by rotating the entire image by any multiple of  $90^\circ$ . However, while robustness can be considerably increased thanks to the use of data augmentation, it is obvious that the model will learn the equivariance instead of being constrained to be rotation equivariant. Unfortunately, this does not lead to any formal guarantee of equivariance and has severe limitations from an efficiency point of view.

Regarding the second category, the most famous method is probably group-CNN by Cohen & Welling (2016). In group-CNN, filters are artificially duplicated in several versions with the application of all the transformations from the considered discrete symmetry group. For example, if the group  $C_4$  (all the rotations for  $\alpha \in \{0, 90^\circ, 180^\circ, 270^\circ\}$ ) is considered, the final number of filters will be multiplied by four after performing  $90^\circ$ ,  $180^\circ$  and  $270^\circ$  rotations on the initial filters. In other words, filters are learned in the same fashion as for vanilla CNN. Yet, when forwarding an input image, each filter is artificially duplicated according to the transformations contained in the considered symmetry group and convolved with the image. At the end of the method, a symmetry pooling is performed to summarize the activations of the different variants of the same filters. Only one copy of each filter needs to be updated during the back-propagation. They are thus defined as real trainable parameters.

Finally, for the third category, general- $E(2)$ -equivariant CNNs ( $E(2)$ -CNNs) by Weiler & Cesa (2019) have become the primary method, achieving equivariance to continuous groups through a finite set of irreducible representations. The idea is closely related to that of steerable filters (Cohen & Welling, 2017; Weiler et al., 2018; Graham et al., 2020), which is widespread in the equivariant CNNs literature. Regarding general- $E(2)$ -equivariant CNNs, they build on the fact that any representation of a finite or compact group can be decomposed into a direct sum of irreducible representations. This decomposition in irreducible representations can be used afterward to constrain the filters. This idea has the advantage of being very general. However, the authors report that irreducible representation for  $SO(2)$  or  $O(2)$  generally does not lead to better performance than the discrete versions  $C_n$  or  $D_n$ .

In this work, we focus on the group-CNN (Cohen & Welling, 2016) method from the second category. This choice is motivated by the fact that methods from the first one do not provide any guarantees on the property of equivariance. With these methods, one cannot be confident in the fact that any trained model fully relies on rotation equivariant features. Methods from the third category, like general- $E(2)$ -equivariant CNNs, are not selected either. This exclusion is based on previous results in the literature showing that approximating the continuous equivariance with a discrete one is most of the time a good solution, and the use of groups (such as  $C_4$ ) is less computationally expensive (Weiler & Cesa, 2019; Delchevalerie et al.,

2023). Consequently, we choose to use the publicly available and general implementation of  $E(2)$ -CNNs<sup>1</sup> that easily allows to build group-CNNs by leveraging discrete symmetry groups.

### 3 Related Work

Exploiting rotation equivariance has been extensively studied for many classification tasks. A non-exhaustive subset of those application domains includes medical imaging Oreiller et al. (2022); Elaldi et al. (2024), microscopic imaging (Chidester et al., 2019b; Graham et al., 2020), satellite imaging (Marcos et al., 2018; Li et al., 2020) or industry 4.0 (Marcos et al., 2016). However, a limited number of works try to address segmentation tasks while applying rotation equivariance constraints.

To the best of our knowledge, the first study to consider exploiting rotation equivariance in U-Net architecture is the work of Chidester et al. (2019a). In their work, the authors investigate the use of group convolutions (restricted to the use of the  $C_4$  group) in a U-Net architecture for nucleus segmentation in histopathological images. The authors conclude that using equivariance to rotations of  $90^\circ$  “enables the network to learn better parameters that generalize well to simple transformations, namely, translations and rotations”.

Other works have considered the use of rotation equivariance, such as the works of Mitton & Murray-Smith (2021) and Oreiller et al. (2022). In the first one, group-CNN are used for a very specific task, deforestation segmentation, while the second one introduces a specific locally rotation invariant bispectral U-Net for the task of multi-organ nucleus segmentation.

Having considered those previous works, we believe that integrating rotation equivariance into CNNs remains under-explored and has to be further researched, more particularly for segmentation tasks using U-Net architectures. The few previous works only investigate one particular configuration for rotation equivariance, and only tackle one specific task. The current literature lacks insights and thorough evaluations of the performance trade-offs and sustainability assessment in terms of computational costs involved in incorporating rotation equivariance into U-Net for segmentation across diverse datasets. The aim of the present work is to close this gap by delivering a more comprehensive assessment of the effectiveness of rotation equivariant U-Net models across various segmentation tasks, while shedding more light on the use of rotation equivariant constraints. By evaluating both rotation-sensitive and standard datasets, we not only investigate the usefulness of rotation equivariance for tasks inherently linked to orientation arbitrariness, but also consider its potential advantages for segmentation tasks that are more general.

### 4 Datasets and Models

This work aims to assess the effectiveness of equivariant U-Net models under several practical conditions: nature of the selected task, dataset size, number of classes for the segmentation task, and model size (number of trainable parameters). First, one can train U-Net models on datasets dealing with tasks of different nature. Either those tasks involve a notion of rotation invariance either at global or local scales (e.g., polyp segmentation mask) or they do not (e.g., segmentation mask of a pedestrian). Second, the selection of datasets is performed such that smaller and larger data regimes exist. Indeed, the usefulness of equivariant constraints may depend on the quantity of available data for training (Delchevalerie et al., 2023). For this reason, in addition to the use of datasets of different sizes, we also consider using different amount of data for each dataset. Third, both binary (one foreground class and one background class) and semantic segmentation (involving a small to large number of distinct classes) are considered. Last, one can consider smaller and larger U-Net models in terms of number of trainable parameters. This is motivated by the idea that equivariant models are constrained by a prior knowledge, which may reduce their required number of parameters to obtain a model with similar performance. In agreement with the aforementioned prerequisites, this section presents the datasets as well as the different architectures considered in this work.

<sup>1</sup><https://github.com/QUVA-Lab/e2cnn>

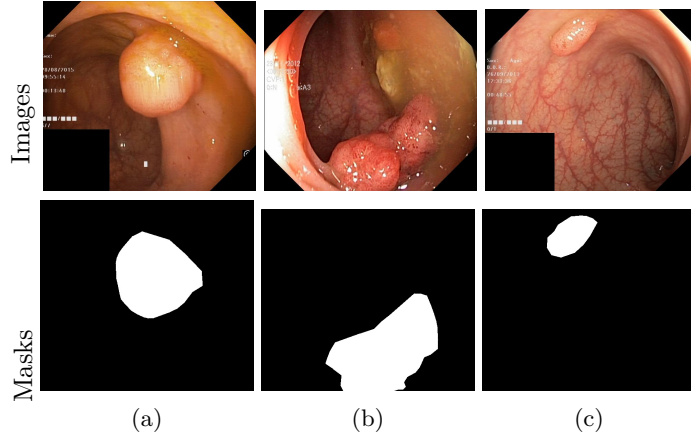


Figure 2: Example of colonoscopy images with their segmentation mask from the Kvasir-SEG dataset. One can notice that the polyps vary in shape and size, and are located at different positions within the images.

#### 4.1 Datasets

Five datasets are considered in this work. The first three datasets are designed for binary segmentation tasks, i.e., masks only contain a foreground and a background. Those datasets are Kvasir-SEG (Jha et al., 2020), NucleiSeg (Janowczyk & Madabhushi, 2016), and URDE (De Silva et al., 2023). Two additional datasets are selected for semantic segmentation, namely COCO-Stuff (Caesar et al., 2018) and iSAID (Waqas Zamir et al., 2019). While the COCO-Stuff is much larger in size than those from the first category, iSAID has the same order of magnitude in terms of image counts. In addition, these datasets are much more general than the first three and are often used as baseline datasets for benchmarking segmentation models. Further, the number of classes that are featured in these two last datasets is greater than in the first three datasets. Also, some datasets feature objects for which the orientation does not matter (like a polyp in Kvasir-SEG), as opposed to other datasets (e.g., a train in COCO-Stuff). Consequently, these five datasets cover a large spectrum of segmentation tasks: smaller/larger datasets, binary/semantic segmentation, and rotation invariant/standard applications. Table 1 presents a summary of key information about each dataset, i.e., the number of images that it contains, images resolution, and the intended use case for the dataset. The next part of this section provides more practical information about them.

**Kvasir-SEG** This first dataset (Jha et al., 2020) contains endoscopic images. Its focus is on the segmentation of polyps in human colons. It contains 1,000 images with varying sizes, from  $625 \times 513$  pixels for the smallest image to  $1920 \times 1072$  pixels for the largest one. Each image is assigned to a binary mask that shows the items of interest, i.e., the polyps. Figure 2 presents three examples of paired images and masks in the dataset. This dataset is expected to be very informative on the ability of a model to learn from only a few images. Furthermore, the task is inherently rotation equivariant, as polyps may appear with any arbitrary orientation.

**NucleiSeg** This second dataset (Janowczyk & Madabhushi, 2016) is designed for segmenting cell nuclei in histopathological images. It contains 135 images with multiple nuclei per image. Each image has a resolution of  $2,000 \times 2,000$  pixels, much more than images from the other binary segmentation datasets considered in this work. Because of this, each image is pre-processed to generate a set of lower resolution images by extracting random patches of  $448 \times 448$  pixels within the original images and masks. Because there are multiple nuclei in each image, the pre-processing will generate sub-images containing multiple nuclei too, such that the images remain useful for the segmentation task. For each image-patch pair, this operation is repeated 30 times to ensure diversity and comprehensiveness. Figure 3 illustrates a few paired image-mask examples resulting from the pre-processing. The NucleiSeg dataset is considered to be informative on the performance of segmentation models in biomedical images having many foreground items per image. The

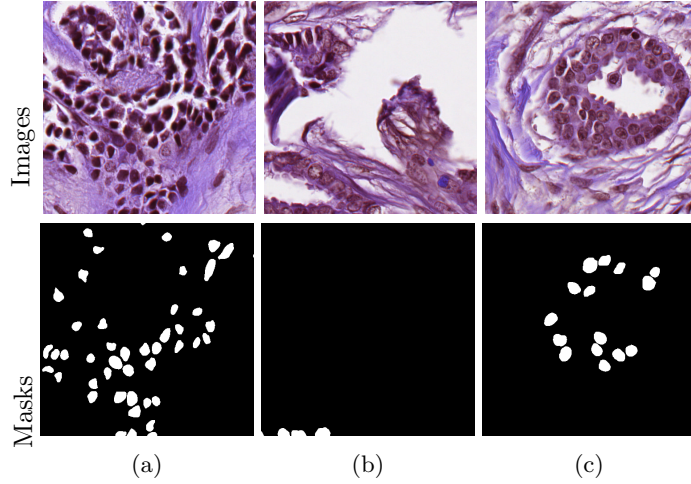


Figure 3: Example of images with their segmentation mask from the NucleiSeg dataset. Notice the multiplicity of nuclei in single patched images.

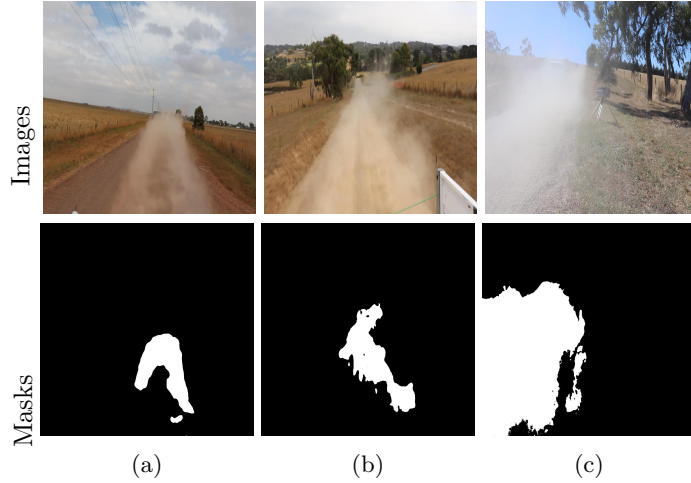


Figure 4: Example of images with their segmentation mask from the URDE dataset. One can notice that the masks have a cloudy, irregular structure.

orientation of the object is not expected to contain any information and objects of interest are always with a circular shape.

**URDE** The name of this third dataset, URDE (De Silva et al., 2023), stands for Urban Roadside Environment and is the last involving binary segmentation. The dataset focuses on detecting dust clouds induced by vehicles traveling on unsealed roads. It includes 7,000 images of  $1,024 \times 1,024$  pixels with their annotation masks. For illustration, Figure 4 presents a sample of paired images and masks in the dataset. In this case, the problem is more general and orientation may be seen as a particular form of information.

**COCO-Stuff** This fourth dataset (Caesar et al., 2018) is a large-scale dataset commonly used for general segmentation tasks. It includes over 164,000 images with 91 stuff categories (plus one class unlabeled) as annotation masks, providing a diverse and extensive set of images for evaluating general-purpose segmentation algorithms. The resolutions vary between images, with a maximum of  $640 \times 640$  pixels. Figure 5 presents a few examples of paired images and masks in the dataset. The complexity and size of the dataset make it a must-have for benchmarking semantic segmentation tasks. Again, as for the URDE dataset, the orientation is not supposed to be meaningless, but in fact can contain meaningful information.



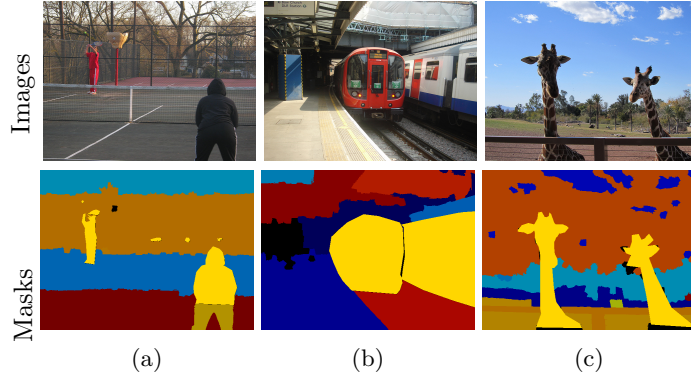


Figure 5: Example of images with their segmentation mask from the COCO-Stuff dataset. Those images illustrate the fact that orientation may matter. For instance, tennis players are expected to be standing up.

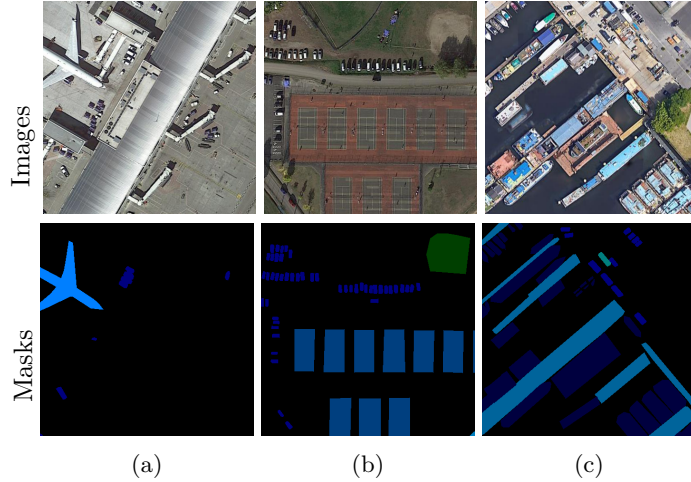


Figure 6: Example of images with their segmentation mask from the iSAID dataset. The orientation in those images does not matter as they are taken from an aerial perspective.

**iSAID** This fifth and last dataset (Waqas Zamir et al., 2019) is based on the DOTA Xia et al. (2018) dataset. While the latter focuses on object detection in satellite imagery, the former focuses on segmentation of the same images. iSAID consists of 2,806 images with annotations for 15 different object classes such as buildings, vehicles, and vegetation. The resolutions of the images vary from  $353 \times 278$  pixels for the smallest image to  $4,294 \times 4,000$  pixels for the largest one. Consequently, the same pre-processing as the one described for the NucleiSeg dataset is applied to initial images and masks as to generate input images and masks of  $448 \times 448$  pixels, 30 times per initial pair of image and mask. In a similar fashion as for other datasets, a few examples of paired images and masks contained in the dataset are presented in Figure 6. For this last dataset, the global orientation of the images is inherently arbitrary and does not carry meaningful information. To illustrate this, one can inspect Figure 6 (b), where the cars (dark blue segmentation masks) appear in different orientations across the image. Indeed, cars at the top of the image have a given orientation, while cars on the bottom-left have a different orientation. The variability in orientation for the same kind of objects is natural for aerial imagery, where objects photographed from above can appear rotated at any angle, but they are in fact the same object. This is exactly the idea captured by the property of rotation equivariance.



Table 1: Dataset Characteristics

Dataset	N. images	Resolution (pixels)	Use Case	Orientation Sensitive
Kvasir-SEG	1,000	$332 \times 487$ to $1,920 \times 1,072$	Polyp segmentation.	×
NucleiSeg	135	$2,000 \times 2,000$	Cell nuclei segmentation.	×
URDE	7,000	$1,024 \times 1,024$	Roadside cloud dust segmentation.	✓
COCO-Stuff	164,000	$59 \times 72$ to $640 \times 640$	General object segmentation.	✓
iSAID	2,806	$353 \times 278$ to $4,294 \times 4,000$	Segmentation in satellite imagery.	×

## 4.2 Model Architectures

After introducing the considered datasets, this section continues with a presentation of U-Net models that are used in this work and the motivation for their selection. These models can be divided in two main categories: (i) vanilla U-Nets and (ii) equivariant U-Nets. For each category, two variations are considered, i.e., large and small models having different magnitude in terms of trainable parameters. Furthermore, several ways of introducing the equivariance into U-Net are considered. To ensure a fair comparison, all models (and all variations of those models) share the same overarching architecture, with differences only in the convolutional approach, and in the number of filters in each layer (in order to compare models with the same number of trainable parameters). The following gives more details about the two categories of U-Net models.

**Vanilla U-Net** The vanilla U-Net serves as the baseline model in this study. U-Net by Ronneberger et al. (2015) is a well-established Convolutional Neural Network (CNN) architecture, commonly used for image segmentation tasks (more details are presented in Section 2). This network relies on standard convolutional layers that are not inherently equivariant to rotations. As a result, this model serves as a baseline to measure the potential benefits of including rotation-equivariant mechanisms in alternative models. As indicated above, a small and a large version of this vanilla U-Net are developed.

The architecture of the vanilla U-Net is close to the one from the original paper by Ronneberger et al. (2015). It is made of two convolutional layers, followed by four down sampling (downsampling is achieved through max pooling layers that divide the resolution by a factor 2) and four up scaling blocks (with bilinear upsampling that increases back the resolution by a factor 2, followed by convolution layers). Note that the use of a bilinear upsampling followed by a convolution is not the most common choice. Most of the time, transposed convolutions (or up-convolutions) are considered instead. However, those layers are not available in the case of equivariant models. Consequently, to ensure a fair comparison, transposed convolution are replaced by this two steps process of an upsampling followed by a simple convolution. In practice, replacing the transposed convolution by this process does not significantly affect the performance and involves the same number of trainable parameters.

All the convolutions in the model use a kernel size of  $3 \times 3$ , and are followed by batch normalization layers and ReLU (Nair & Hinton, 2010) activation functions. The first convolutional layer takes a fixed  $224 \times 224$  input images. Finally, the last convolutional layer reduces the number of channels to the number of classes that are to be predicted.

All the elements regarding the U-Net configuration that are described in the previous paragraph are common for the two vanilla U-Net models (small and large), but they count a different number of trainable parameters. The small model is made of roughly 500,000 trainable parameters, while the large one counts roughly 11,000,000 of them. In order to create differences in models size, a factor  $\lambda \in \mathbb{R}$  is introduced to divide the number of filters in each layer of the model, thereby controlling the number of trainable parameters in the model.  $\lambda$  has a constant, specific value for each model and size combination. For example,  $\lambda = 1.65$  for the large vanilla U-Net, and 6.00 for its small counterpart. The final number of filters for each convolutional layer is found in Table 2.

**E(2)-U-Net** The  $E(2)$ -U-Net modifies the vanilla U-Net architecture by incorporating equivariant convolutional blocks. Those equivariant convolutional blocks follow the exact same architecture as for the vanilla U-Net, except that the group convolution implemented in  $E(2)$ -CNNs (Weiler & Cesa, 2019) is used. In

Table 2: Number of filters for the different models, for the two first convolutional layers (conv1, conv2), the four downsampling blocks (D1, D2, D3, D4, located on the left-hand side of Figure 1), and upsampling blocks (U1, U2, U3, U4, presented on the right-hand side of Figure 1).

	Small Models										Large Models									
	conv1	conv2	D1	D2	D3	D4	U1	U2	U3	U4	conv1	conv2	D1	D2	D3	D4	U1	U2	U3	U4
<b>vanilla</b>	12	12	22	44	86	172	86	44	22	12	52	52	104	206	410	820	410	206	104	52
<b>C4</b>	4	4	6	12	24	46	24	12	6	4	14	14	28	56	112	222	112	56	28	14
<b>C8/D4</b>	4	4	6	10	18	34	18	10	6	4	10	10	20	40	78	154	78	40	20	10

addition, modified versions of ReLU activation functions and batch-normalization layers are also used. This is necessary given the fact that  $E(2)$ -CNNs involve a particular representation of the data that require using specific activation functions and normalization. Furthermore, a final layer is also added at the end of the decoder part to perform the symmetry pooling over the different transformations in the considered symmetry group (see Section 2 for more details). Finally, an important modification is also the use of bigger filter sizes compared to vanilla convolutions. Indeed, many previous work on equivariant CNNs (Weiler & Cesa, 2019; Worrall et al., 2017; Delchevalerie et al., 2023) show that using larger filter sizes is required to be able to achieve rotation equivariance (due to the use of a cartesian grid to represent images). This results in  $E(2)$ -U-Nets using a kernel size of  $9 \times 9$  for convolutions, instead of  $3 \times 3$  for the vanilla counterpart.

Similarly to the vanilla U-Net, small and large versions of the models are defined by modifying the number of filters in each layer. Additionally, several symmetry groups are considered per  $E(2)$ -U-Net model:

- $C_4$ : the cyclic group of order 4, which ensures equivariance to rotations of  $90^\circ$ .
- $C_8$ : the cyclic group of order 8, which extends equivariance to rotations of  $45^\circ$ .
- $D_4$ : the dihedral group of order 4, which combines  $90^\circ$  rotations and reflections.

This setup results in the creation of six  $E(2)$ -U-Net architectures (three small, and three large models). All the configurations are presented in Table 2, together with the number of filters in each layer.

## 5 Experiments

This section deals with the experiments performed in this study. First, the training setup is outlined, with details on the selected optimizer, loss function, and their hyperparameters. Second, details about the evaluation metrics for each task are presented. Third, the results obtained by the vanilla U-Net as well as the different  $E(2)$ -U-Net models across the different tasks are presented.

### 5.1 Training Setup

All models are trained under identical conditions to ensure a fair comparison. The selection of hyperparameters is based on the initial paper of each dataset, except for NucleiSeg, where the author’s implementation deviated too much from approaches used in the four other datasets. Indeed, the authors use a batch size of 128 of patched images having a size of  $32 \times 32$  pixels and train their model over 600,000 steps (Janowczyk & Madabhushi, 2016). Because our model accepts images with input size of 224, the resolution chosen by the authors is too small for our study. As a consequence, standard hyperparameters are retained for this dataset. The AdamW (Loshchilov & Hutter, 2019) optimizer is selected for all datasets, with a learning rate and a number of epoch that is specific to each dataset, as presented in Table 3. The Dice Loss (Sudre et al., 2017) is retained as the only loss criterion, because it is well-suited for segmentation tasks, in particular with imbalanced data. Similarly, the batch size is specific for each dataset and is also indicated in Table 3. Finally, the following data augmentation techniques are applied to images and their corresponding mask during training: random rotations of  $0^\circ, 90^\circ, 180^\circ$  or  $270^\circ$  with probability 0.25 each, horizontal and/or vertical flip(s) with probability 0.5 for each, and also a color normalization.

Table 3: Hyperparameters for Each Dataset

Dataset	Batch Size	Learning Rate	N. epochs
Kvasir-SEG	8	$1 \times 10^{-4}$	150
NucleiSeg	16	$1 \times 10^{-4}$	200
COCO-Stuff	16	$1 \times 10^{-3}$	200
URDE	4	$5 \times 10^{-4}$	500
iSAID	16	$1 \times 10^{-4}$	250

For each model configuration, five-fold cross-validation is used. To do so, the dataset is partitioned into five non-overlapping subsets. For each of the five folds, four subsets are used for training while the remaining one is used for testing. This approach guarantees that each sample appears in the test set exactly once, and provides statistical robustness of the results. As already presented in Section 4, two different quantity of data are considered for training for all the different datasets. Those two settings are defined by (i) “Large data setting” and (ii) “Small data setting” and correspond to the use of the full 4 folds for training for (i) , and the use of only a subset of 10% of each fold for (ii). Thus, (i) corresponds to the use of 80% of the available data for training, while (ii) corresponds to the use of only 8% of the initial dataset (i.e., 10% of the 80% of total data). For both settings, the testing set is held constant, and is the entirety of the remaining fold (made of 20% of the data). All models are trained using one Nvidia Tesla A100 with 40GB.

## 5.2 Evaluation metrics

The performance of the models is evaluated using metrics that are specific to the task at hand: binary segmentation or semantic segmentation.

For the binary segmentation tasks, one must classify each individual pixel as belonging either to the foreground class or to the background class. Five performance metrics are selected to evaluate the ability of a model to correctly identify the foreground class in images.

- **Dice Score (DS)** is a measure of the similarity (or overlap) between two sets, i.e., predicted segmentation masks (P) and ground truth masks (G). DS is computed as the ratio of twice the intersection of the predicted and ground truth masks to the sum of their total pixel counts. A perfect overlap has a DS of 1 since all pixels are forecasted in the correct class, while a DS of 0 means that there is absolutely no overlap between forecasted masks and their ground truth.

$$DS = \frac{2 \times |P \cap G|}{|P| + |G|}$$

- **Intersection over Union (IoU)** measures the overlap between the predicted segmentation masks (P) and their ground truth (G). IoU is defined as the intersection of the predicted and ground truth segments divided by their union.

$$IoU = \frac{|P \cap G|}{|P \cup G|}$$

- **Precision** is the ratio of True Positives (TP) to the sum of TP and False Positives (FP). This metric indicates the ability of a model to avoid false positives: the greater the ratio, the lower the relative FP.

$$\text{Precision} = \frac{TP}{TP + FP}$$

- **Recall** is the ratio of TP to the sum of TP and False Negatives (FN). Recall measures the ability of a model to detect the foreground class.

$$\text{Recall} = \frac{TP}{TP + FN}$$

- **Accuracy** is the proportion of correctly classified pixels, i.e., TP and True Negatives (TN) out of the total number of pixels.

$$\text{Accuracy} = \frac{TP + TN}{TP + TN + FP + FN}$$

In order to assess the performance of the models on the semantic segmentation tasks, four widely used evaluation criteria are selected Caesar et al. (2018); Long et al. (2015); Eigen & Fergus (2015); Caesar et al. (2016): (i) Mean Intersection over Union (mIoU) divides how many pixels are in the intersection between predictions and ground-truth class, and average the number over classes, (ii) Frequency-weighted IoU (FW IoU) is the per-class IoU, weighted by the frequency (at the pixel-level) of each class, (iii) Mean Accuracy (mAcc), is the average average pixel accuracy calculated across all classes, and (iv) Pixel Accuracy (pAcc) is the percentage of pixels that are correctly labeled. Note that these criteria are derived from binary segmentation metrics described above.

### 5.3 Results

This section presents the results obtained for the five datasets. For each of them, the results for the small and large models, both for the vanilla and  $E(2)$ -U-Net are presented. Each configuration has two settings: a small data setting (i.e., only 10% of each training fold is used), and a large data setting (i.e., the full 4 folds are used for training). This means that for each dataset, each of the four models (one vanilla, and three  $E(2)$ -U-Net) has four variations: small/large number of trainable parameters (two variations), and small/large data setting (two additional variations). This resulted in the training of 16 models, for each of the five datasets.

**Kvasir-SEG** Results for the Kvasir-SEG dataset are summarized in Table 4. In large data setting, and regarding the small models, the  $E(2)$ -U-Net model based on the use of the  $C_8$  symmetry group outperforms the others in terms of Dice Score, IoU, precision, and accuracy, whereas the vanilla U-Net achieves the highest recall. Regarding the larger models for the same data setting, the  $E(2)$ -U-Net based on  $C_8$  again shows the best performance in Dice Score, IoU, accuracy, and recall. With regards to precision, both  $C_8$  and  $D_4$  show comparable performances. In small data setting, the small models show better Dice Score, IoU, precision, and accuracy for  $C_8$  while  $C_4$  has the highest recall. As far as the large models and small data setting is concerned, the overall picture is comparable to that of the small models for the same data setup in terms of DS and IoU, where  $C_8$  has the highest metrics. Interestingly, the vanilla model has the best recall for the large model. Overall, the equivariant models show better performances than the vanilla counterparts, both regarding small and large models.

Table 4: Performance metrics for the Kvasir-SEG dataset

Model	Large data setting					Small data setting				
	Dice	IoU	Pre.	Rec.	Acc.	Dice	IoU	Pre.	Rec.	Acc.
<b>Small models</b>										
<i>vanilla</i>	80.5 $\pm$ 2.5	68.0 $\pm$ 3.1	79.2 $\pm$ 6.1	<b>83.5</b> $\pm$ 4.4	93.9 $\pm$ 1.2	54.4 $\pm$ 6.7	38.0 $\pm$ 6.0	65.4 $\pm$ 13.3	52.6 $\pm$ 11.1	87.2 $\pm$ 2.8
$C_4$	80.6 $\pm$ 3.2	68.3 $\pm$ 4.3	84.2 $\pm$ 3.8	79.2 $\pm$ 4.4	94.2 $\pm$ 1.1	50.5 $\pm$ 9.5	35.3 $\pm$ 7.9	55.0 $\pm$ 14.7	<b>63.1</b> $\pm$ 14.0	72.9 $\pm$ 20.2
$C_8$	<b>83.1</b> $\pm$ 2.9	<b>71.8</b> $\pm$ 4.0	<b>86.7</b> $\pm$ 1.5	81.2 $\pm$ 5.3	<b>95.0</b> $\pm$ 0.9	<b>60.4</b> $\pm$ 2.6	<b>44.1</b> $\pm$ 2.6	<b>74.9</b> $\pm$ 8.3	53.0 $\pm$ 5.0	<b>89.6</b> $\pm$ 0.5
$D_4$	81.1 $\pm$ 3.6	69.0 $\pm$ 4.8	85.0 $\pm$ 4.5	79.0 $\pm$ 5.0	94.4 $\pm$ 1.3	49.8 $\pm$ 9.2	34.7 $\pm$ 8.0	57.6 $\pm$ 14.9	59.0 $\pm$ 15.4	74.0 $\pm$ 20.0
<b>Large models</b>										
<i>vanilla</i>	86.5 $\pm$ 1.6	76.7 $\pm$ 2.3	89.5 $\pm$ 1.1	84.7 $\pm$ 2.7	96.0 $\pm$ 0.5	66.5 $\pm$ 3.8	50.8 $\pm$ 4.1	76.2 $\pm$ 5.8	<b>61.3</b> $\pm$ 9.9	90.7 $\pm$ 0.4
$C_4$	87.2 $\pm$ 1.2	77.8 $\pm$ 1.7	88.8 $\pm$ 2.0	86.6 $\pm$ 1.7	96.2 $\pm$ 0.4	66.7 $\pm$ 3.3	51.1 $\pm$ 3.5	<b>83.9</b> $\pm$ 5.0	57.4 $\pm$ 3.7	91.4 $\pm$ 0.5
$C_8$	<b>88.0</b> $\pm$ 1.9	<b>79.0</b> $\pm$ 2.8	<b>90.2</b> $\pm$ 1.2	<b>86.8</b> $\pm$ 3.4	<b>96.4</b> $\pm$ 0.7	<b>68.3</b> $\pm$ 3.9	<b>53.0</b> $\pm$ 4.7	82.7 $\pm$ 2.7	60.0 $\pm$ 4.8	<b>91.7</b> $\pm$ 0.5
$D_4$	86.4 $\pm$ 1.9	76.7 $\pm$ 3.1	<b>90.2</b> $\pm$ 1.6	84.0 $\pm$ 2.7	96.0 $\pm$ 0.7	63.8 $\pm$ 2.7	47.7 $\pm$ 2.8	83.5 $\pm$ 7.4	53.4 $\pm$ 4.5	90.9 $\pm$ 0.6

While the above analysis helps in understanding models’ performance when there is no constraint on training resources, a second analysis is performed to assess the performance from a sustainability standpoint that considers the resources used. To do so, one can visualize the evolution of performance against the cumulative time during training. Therefore, we also present in Figure 7 the IoU with respect to the cumulative training

time (in seconds) for both the large and small models, both for the small and large data setting case. Please note that the total number of epochs is the same for all models and all configurations. Under large data setup in this Figure, one sees the vanilla U-Net is better than the equivariant ones until it stops training at  $3 \times 10^2$  and  $7 \times 10^2$  seconds, for small and large models respectively. Thus, if one had to stop training early, the vanilla model would be better, leading to a gain in computational resources. The same observation can be made about small data setup.

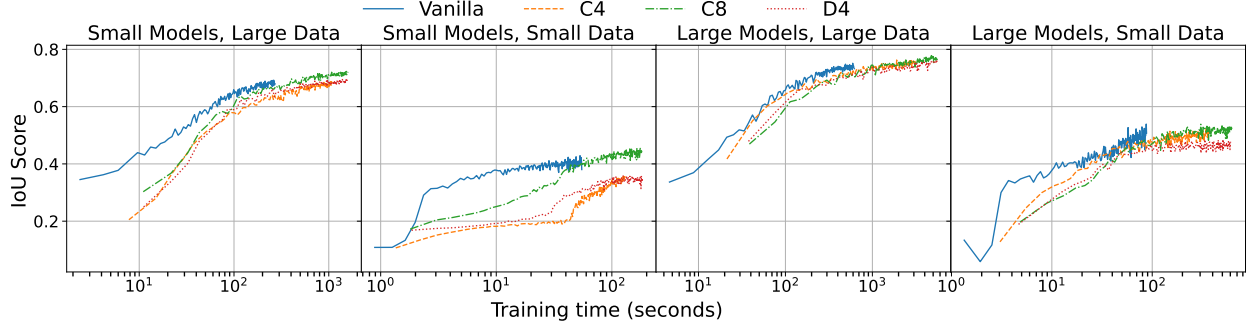


Figure 7: Kvasir-SEG: IoU performance over cumulative time (in seconds) for small and large models in small and large data setting, averaged across the 5 folds. The total number of epochs is the same for all models and all configurations.

**NucleiSeg** Results for the NucleiSeg dataset are summarized in Table 5. Regarding the large data setting for the small models, one can observe that the vanilla U-Net model has the highest Dice Score, IoU and recall. Considering the precision metric, the  $E(2)$ -U-Net based on the  $C_8$  symmetry group achieves the best score. As far as the accuracy is concerned,  $C_8$  and  $D_4$  both show the highest score. For the large data setting and the large models, the vanilla U-Net model has the best Dice Score, IoU, precision, and recall.  $C_4$  has the highest accuracy level. The small data setting reveals that vanilla models for both small and large models have the best Dice Score and IoU. The other metrics are dominated by  $C_8$  or  $D_4$ . Overall, the vanilla models seem to perform better than the equivariant counterparts for this dataset.

Table 5: Performance metrics for the NucleiSeg dataset

Model	Large data setting					Small data setting				
	Dice	IoU	Pre.	Rec.	Acc.	Dice	IoU	Pre.	Rec.	Acc.
<b>Small models</b>										
<i>vanilla</i>	<b>28.4</b> $\pm 7.6$	<b>17.3</b> $\pm 5.1$	37.4 $\pm 3.6$	<b>30.1</b> $\pm 13.8$	97.0 $\pm 0.7$	<b>18.7</b> $\pm 7.3$	<b>10.8</b> $\pm 4.6$	25.2 $\pm 3.2$	20.5 $\pm 10.5$	96.6 $\pm 0.4$
$C_4$	25.7 $\pm 2.8$	15.2 $\pm 1.8$	33.3 $\pm 2.8$	25.0 $\pm 5.5$	97.0 $\pm 0.2$	15.1 $\pm 3.6$	8.4 $\pm 2.0$	27.3 $\pm 2.7$	12.1 $\pm 3.1$	97.2 $\pm 0.3$
$C_8$	23.4 $\pm 4.3$	13.8 $\pm 2.8$	<b>37.8</b> $\pm 3.4$	19.8 $\pm 5.6$	<b>97.3</b> $\pm 0.3$	13.8 $\pm 6.2$	7.7 $\pm 3.7$	<b>30.5</b> $\pm 4.2$	10.4 $\pm 6.0$	<b>97.4</b> $\pm 0.4$
$D_4$	24.5 $\pm 5.2$	14.5 $\pm 3.3$	37.6 $\pm 4.3$	21.2 $\pm 6.9$	<b>97.3</b> $\pm 0.2$	12.9 $\pm 5.9$	7.1 $\pm 3.5$	22.8 $\pm 14.5$	<b>29.2</b> $\pm 9.5$	78.3 $\pm 2.7$
<b>Large models</b>										
<i>vanilla</i>	<b>39.8</b> $\pm 2.3$	<b>25.9</b> $\pm 1.7$	<b>36.9</b> $\pm 1.7$	<b>53.3</b> $\pm 4.7$	96.5 $\pm 0.6$	<b>24.9</b> $\pm 8.3$	<b>15.1</b> $\pm 5.5$	36.1 $\pm 7.1$	<b>26.0</b> $\pm 16.9$	97.0 $\pm 0.8$
$C_4$	34.4 $\pm 1.7$	21.6 $\pm 1.2$	34.8 $\pm 2.3$	40.1 $\pm 5.6$	<b>96.8</b> $\pm 0.5$	15.8 $\pm 3.6$	9.0 $\pm 2.1$	<b>38.4</b> $\pm 1.6$	11.4 $\pm 3.1$	<b>97.5</b> $\pm 0.4$
$C_8$	34.8 $\pm 2.3$	21.8 $\pm 1.9$	34.4 $\pm 3.2$	42.4 $\pm 3.6$	96.7 $\pm 0.4$	14.4 $\pm 4.1$	8.2 $\pm 2.5$	37.4 $\pm 4.0$	10.4 $\pm 4.4$	<b>97.5</b> $\pm 0.4$
$D_4$	33.7 $\pm 3.1$	21.0 $\pm 2.4$	33.3 $\pm 2.6$	43.5 $\pm 6.8$	96.4 $\pm 0.6$	13.0 $\pm 5.2$	7.3 $\pm 3.1$	37.2 $\pm 3.3$	9.2 $\pm 4.4$	<b>97.5</b> $\pm 0.5$

Figure 8 presents the IoU with respect to the cumulative time in seconds (with a constant number of epochs throughout models and setups). It shows that vanilla models have the greatest performance throughout. Also, one can notice that the performance starts dropping around time  $2 \times 10^2$  and  $5 \times 10^2$  seconds for small and large models respectively, under the large data setup. This is also true for the small data setup, with a drop of performance at  $1 \times 10^2$  and  $1 \times 10^2$  seconds.

**URDE** Results for the URDE dataset are summarized in Table 6. Focusing on large data setting and small models, the  $E(2)$ -U-Net based on  $C_4$  and  $D_4$  models achieve comparable Dice and IoU. The  $D_4$  variant also

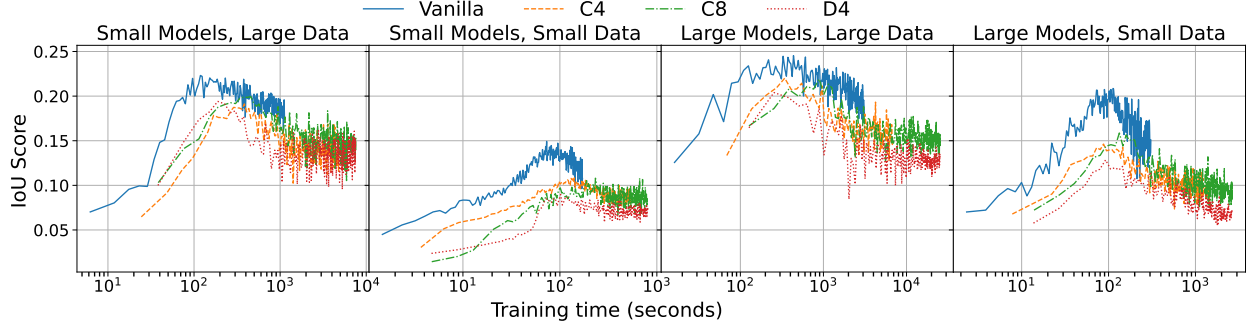


Figure 8: NucleiSeg: IoU performance over cumulative time (in seconds) for small and large models in small and large data setting, averaged across the 5 folds. The total number of epochs is the same for all models and all configurations.

has the highest precision while the  $C_8$  model outperforms the other models in recall. The equivariant configurations all achieve highest accuracy metrics. For the larger models under the large data setting, the  $E(2)$ -U-Net based on  $C_4$  shows the best DS, IoU, precision and recall. It also achieves the highest accuracy, and this score is matched by  $C_8$ . The small data setting shows that the best large model is  $C_4$  for all performance metrics. Regarding the small models of this same setting,  $C_4$  has the highest Dice Score, IoU, recall and accuracy, whereas  $C_8$  has the best precision.

Table 6: Performance metrics for the URDE dataset

Model	Large data setting					Small data setting				
	Dice	IoU	Pre.	Rec.	Acc.	Dice	IoU	Pre.	Rec.	Acc.
<b>Small models</b>										
<i>vanilla</i>	78.1 $\pm$ 2.4	70.9 $\pm$ 2.2	41.4 $\pm$ 3.1	39.3 $\pm$ 3.9	98.5 $\pm$ 0.1	65.9 $\pm$ 4.3	58.6 $\pm$ 4.7	31.7 $\pm$ 3.5	33.2 $\pm$ 4.5	97.9 $\pm$ 0.2
$C_4$	82.0 $\pm$ 1.6	<b>75.0</b> $\pm$ 1.7	43.5 $\pm$ 2.7	42.1 $\pm$ 2.4	<b>98.7</b> $\pm$ 0.1	<b>67.9</b> $\pm$ 2.6	<b>60.4</b> $\pm$ 2.6	37.5 $\pm$ 2.7	<b>33.4</b> $\pm$ 2.3	<b>98.2</b> $\pm$ 0.1
$C_8$	81.6 $\pm$ 2.1	74.7 $\pm$ 2.2	43.5 $\pm$ 2.1	<b>42.3</b> $\pm$ 2.8	98.7 $\pm$ 0.1	66.4 $\pm$ 4.9	58.7 $\pm$ 4.8	<b>37.8</b> $\pm$ 2.5	32.9 $\pm$ 2.0	98.1 $\pm$ 0.1
$D_4$	<b>82.1</b> $\pm$ 1.3	<b>75.0</b> $\pm$ 1.4	<b>44.0</b> $\pm$ 2.2	41.9 $\pm$ 2.7	98.7 $\pm$ 0.1	65.9 $\pm$ 2.9	58.1 $\pm$ 2.9	37.5 $\pm$ 3.0	32.8 $\pm$ 2.6	98.1 $\pm$ 0.1
<b>Large models</b>										
<i>vanilla</i>	81.3 $\pm$ 1.0	74.1 $\pm$ 0.8	42.2 $\pm$ 1.6	40.4 $\pm$ 2.3	98.6 $\pm$ 0.1	62.1 $\pm$ 8.4	54.8 $\pm$ 8.8	32.4 $\pm$ 1.9	32.0 $\pm$ 3.5	97.7 $\pm$ 0.5
$C_4$	<b>84.4</b> $\pm$ 1.5	<b>77.6</b> $\pm$ 1.4	<b>44.6</b> $\pm$ 1.9	43.0 $\pm$ 3.3	<b>98.8</b> $\pm$ 0.1	<b>71.3</b> $\pm$ 2.2	<b>63.5</b> $\pm$ 1.9	<b>39.1</b> $\pm$ 3.2	<b>33.4</b> $\pm$ 2.9	<b>98.2</b> $\pm$ 0.1
$C_8$	83.6 $\pm$ 1.6	76.6 $\pm$ 1.6	43.2 $\pm$ 1.8	<b>43.1</b> $\pm$ 3.3	<b>98.7</b> $\pm$ 0.1	70.6 $\pm$ 2.9	63.0 $\pm$ 2.9	38.0 $\pm$ 1.7	33.1 $\pm$ 1.5	<b>98.2</b> $\pm$ 0.1
$D_4$	84.2 $\pm$ 1.5	77.2 $\pm$ 1.4	44.5 $\pm$ 2.2	42.8 $\pm$ 2.7	<b>98.7</b> $\pm$ 0.1	71.0 $\pm$ 1.9	63.2 $\pm$ 1.9	38.6 $\pm$ 2.5	32.9 $\pm$ 1.2	98.1 $\pm$ 0.0

Now regarding the time-performance plot (with the same total number of epochs for all configurations and models) presented in Figure 9, it clearly appears that for the small data setting as well as for the large data setting, the vanilla U-Net is significantly below the three equivariant models in terms of IoU, both for the small and large models.

**COCO stuff** Results for the COCO-Stuff dataset are presented in Table 7. For small models in large data setting, the vanilla U-Net shows better performances than the  $E(2)$ -U-Nets for all metrics, except for mean accuracy, where its performance is equal to that of  $C_4$ . However, when considering larger models,  $C_4$  and  $C_8$  models close the gaps in performances and  $C_8$  even achieve the best mean IoU and mean accuracy. The  $D_4$  model seems always under in terms of performance metrics. In small data setting however, the vanilla model is best across all metrics, both for small and large models.

The analysis of Figure 10 (similarly as the similar analyses, total number of epochs is constant) shows that under the large data setting, the small vanilla model is always better than its equivariant counterparts in terms of mean IoU. However, when looking at large models, it is not always the case. Indeed, between times  $1.5 \times 10^3$  and  $8 \times 10^4$ , one notices that very similar performances between vanilla and  $C_4$  models. In the end,

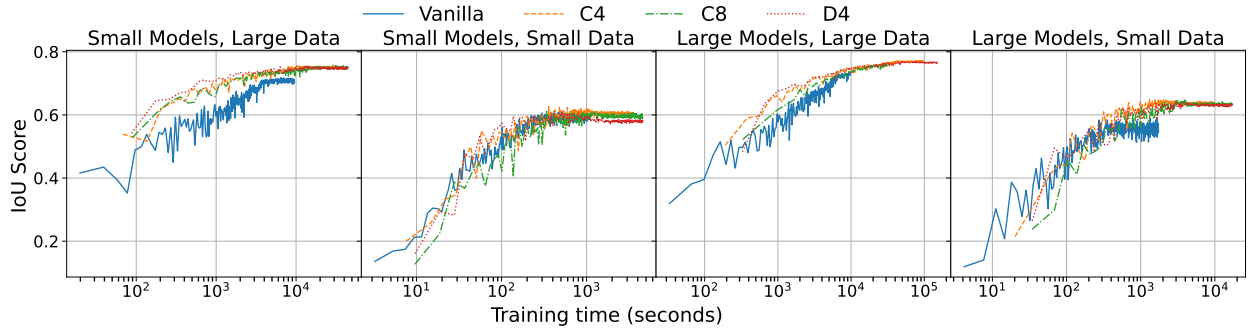


Figure 9: URDE: IoU performance over cumulative time (in seconds) for small and large models in small and large data setting, averaged across the 5 folds. The total number of epochs is the same for all models and all configurations.

Table 7: Performance metrics for the COCO-Stuff dataset

Model	Large data setting				Small data setting			
	Mean IoU	Pixel Acc.	Mean Acc.	fW IoU	Mean IoU	Pixel Acc.	Mean Acc.	fW IoU
<b>Small models</b>								
<i>vanilla</i>	<b>13.6</b> $\pm 0.2$	<b>64.2</b> $\pm 0.3$	<b>18.9</b> $\pm 0.2$	<b>49.1</b> $\pm 0.5$	<b>10.8</b> $\pm 0.2$	<b>60.1</b> $\pm 0.3$	<b>15.7</b> $\pm 0.3$	<b>44.6</b> $\pm 0.6$
$C_4$	13.5 $\pm 0.1$	64.0 $\pm 0.3$	<b>18.9</b> $\pm 0.2$	48.9 $\pm 0.5$	9.5 $\pm 0.2$	56.9 $\pm 0.4$	14.1 $\pm 0.2$	41.4 $\pm 0.4$
$C_8$	13.0 $\pm 0.6$	63.0 $\pm 1.0$	18.4 $\pm 0.9$	47.7 $\pm 1.4$	9.6 $\pm 0.3$	57.6 $\pm 0.4$	14.3 $\pm 0.3$	42.6 $\pm 0.3$
$D_4$	12.9 $\pm 0.5$	62.9 $\pm 0.7$	18.2 $\pm 0.6$	47.4 $\pm 0.9$	8.6 $\pm 0.3$	55.1 $\pm 0.7$	12.7 $\pm 0.3$	40.9 $\pm 0.6$
<b>Large models</b>								
<i>vanilla</i>	17.9 $\pm 0.1$	<b>68.9</b> $\pm 0.2$	23.8 $\pm 0.3$	<b>56.3</b> $\pm 0.6$	<b>10.9</b> $\pm 0.3$	<b>60.9</b> $\pm 0.4$	<b>15.2</b> $\pm 0.4$	<b>47.7</b> $\pm 0.5$
$C_4$	18.2 $\pm 0.2$	67.8 $\pm 0.2$	24.1 $\pm 0.2$	54.8 $\pm 0.3$	10.6 $\pm 0.3$	60.4 $\pm 0.4$	14.9 $\pm 0.3$	47.2 $\pm 0.4$
$C_8$	<b>18.3</b> $\pm 0.4$	67.8 $\pm 0.2$	<b>24.2</b> $\pm 0.6$	54.8 $\pm 0.7$	10.4 $\pm 0.1$	60.3 $\pm 0.3$	14.5 $\pm 0.1$	47.2 $\pm 0.1$
$D_4$	16.7 $\pm 0.3$	65.9 $\pm 0.5$	22.5 $\pm 0.2$	53.4 $\pm 0.1$	9.1 $\pm 0.2$	58.7 $\pm 0.4$	12.9 $\pm 0.3$	45.6 $\pm 0.5$

$C_4$  and  $C_8$  finish at higher mean IoU levels than the vanilla U-Net. For the small data setup, the vanilla model is always the best in terms of mean IoU.

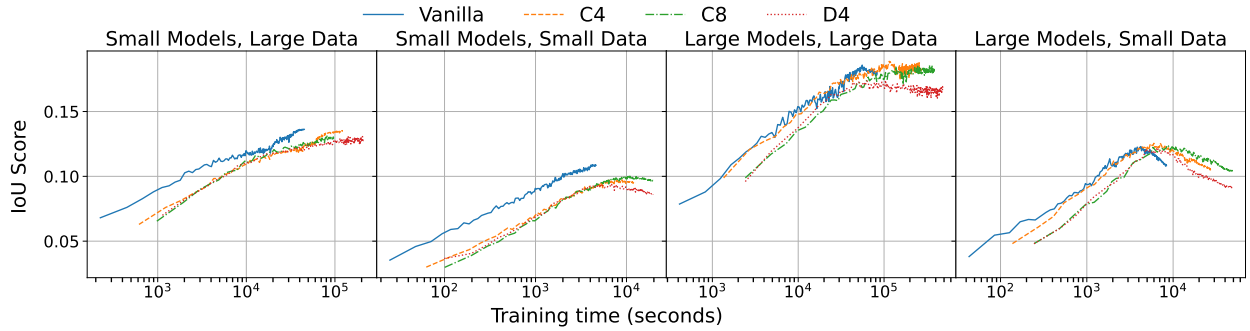


Figure 10: COCO-Stuff: mean IoU performance over cumulative time (in seconds) for small and large models in small and large data setting, averaged across the 5 folds. The total number of epochs is the same for all models and all configurations.



**iSAID** Results for the iSAID dataset are presented in Table 8. As far as both the small and large data setting are concerned, and for both the small and large models, the vanilla U-Net outperforms the three others across all metrics, with a clear outperformance regarding the mean IoU and the mean accuracy.

Table 8: Performance metrics for the iSAID dataset

Model	Large data setting				Small data setting			
	Mean IoU	Pixel Acc.	Mean Acc.	fW IoU	Mean IoU	Pixel Acc.	Mean Acc.	fW IoU
<b>Small models</b>								
<i>vanilla</i>	<b>39.9</b> $\pm 1.6$	<b>97.2</b> $\pm 0.3$	<b>43.5</b> $\pm 1.7$	<b>95.1</b> $\pm 0.4$	<b>30.3</b> $\pm 1.7$	<b>95.9</b> $\pm 0.5$	<b>33.3</b> $\pm 1.8$	<b>93.1</b> $\pm 0.8$
$C_4$	33.4 $\pm 2.6$	96.8 $\pm 0.3$	36.7 $\pm 2.8$	94.5 $\pm 0.4$	23.5 $\pm 1.2$	95.1 $\pm 0.4$	25.8 $\pm 1.2$	91.9 $\pm 0.7$
$C_8$	34.9 $\pm 2.0$	97.1 $\pm 0.2$	38.6 $\pm 1.9$	94.9 $\pm 0.4$	24.6 $\pm 2.0$	95.6 $\pm 0.3$	27.1 $\pm 1.9$	92.6 $\pm 0.5$
$D_4$	30.8 $\pm 2.9$	96.8 $\pm 0.3$	34.1 $\pm 3.2$	94.4 $\pm 0.5$	20.3 $\pm 1.2$	95.0 $\pm 0.4$	22.4 $\pm 1.3$	91.7 $\pm 0.7$
<b>Large models</b>								
<i>vanilla</i>	<b>48.2</b> $\pm 1.8$	<b>97.6</b> $\pm 0.3$	<b>52.7</b> $\pm 1.7$	<b>95.8</b> $\pm 0.4$	<b>36.2</b> $\pm 2.0$	<b>96.9</b> $\pm 0.3$	<b>39.7</b> $\pm 2.0$	<b>94.6</b> $\pm 0.4$
$C_4$	43.1 $\pm 1.6$	97.5 $\pm 0.2$	47.1 $\pm 1.7$	95.5 $\pm 0.4$	32.1 $\pm 1.0$	96.3 $\pm 0.3$	35.0 $\pm 1.0$	93.6 $\pm 0.5$
$C_8$	44.6 $\pm 1.4$	97.6 $\pm 0.3$	48.8 $\pm 1.6$	95.7 $\pm 0.4$	32.3 $\pm 1.0$	96.5 $\pm 0.3$	35.2 $\pm 1.0$	93.9 $\pm 0.5$
$D_4$	40.4 $\pm 0.2$	97.3 $\pm 0.3$	44.2 $\pm 0.2$	95.3 $\pm 0.4$	26.3 $\pm 0.6$	96.1 $\pm 0.3$	28.7 $\pm 0.8$	93.2 $\pm 0.5$

The analysis of mean IoU against cumulative time (in seconds) in Figure 11 shows that the vanilla models are always the best, for the small and the large data setup, both for small and large models.

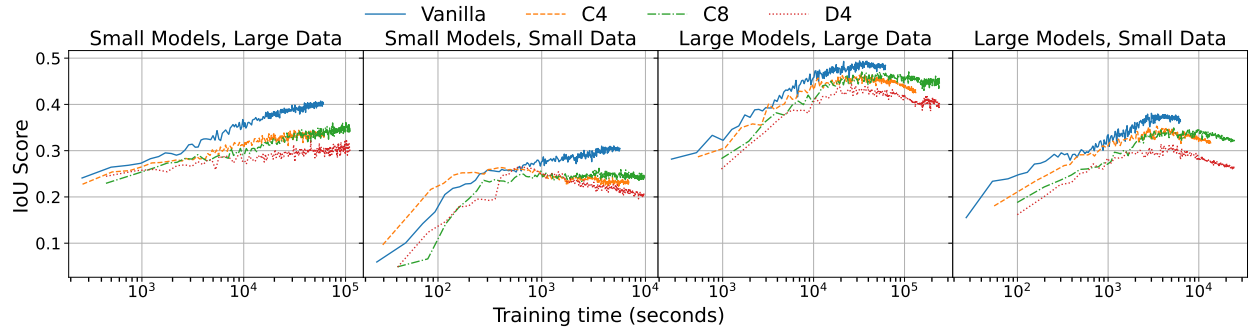


Figure 11: iSAID mean IoU performance over cumulative time (in seconds) for small and large models in small and large data setting, averaged across the 5 folds. The total number of epochs is the same for all models and all configurations.

## 6 Discussion

The analysis of the results reveals interesting patterns regarding the usefulness of equivariant models across the model sizes, the type of tasks, the dataset specificity (i.e., the size, nature of images, and number of classes) and the data regime. This section sums up the observations from the previous section, and try to extract some insights about when it could be interesting to consider equivariant U-Net for segmentation tasks. Based on the results and previous studies in the literature (see Section 2), the discussion is subdivided in two parts, depending on the interest one has in using equivariant models: (i) getting an improvement in terms of evaluation metrics (“are equivariant models better at solving the considered task?”) and (ii) getting an improvement in terms of sustainability (“are equivariant models able to achieve comparable performances while reducing the amount of required computational resources?”).

## 6.1 Discussion based on evaluation metrics

First, we begin by presenting our key findings on evaluation metrics. We then discuss the overall performances independently for the different setups in terms of model size and data regime (small or large). In particular, we discuss performances for (i) small models in large data settings, (ii) large models in large data settings, (iii) small models in small data settings, and (iv) large models in small data settings.

**Key findings** Our analysis reveals that the effectiveness of equivariant U-Net compared to their vanilla counterparts largely depends on the nature of the objects as well as the complexity of the segmentation task. For datasets where objects can have arbitrary shapes, and their orientation is not semantically meaningful, such as Kvasir-SEG and URDE, we find that equivariant models often outperform vanilla architectures (See Table 4 and Table 6). However, when objects are symmetric from a rotational standpoint (e.g., nuclei have circular shapes in NucleiSeg), vanilla U-Nets show better performance than their rotation equivariant counterparts. One explanation is that the rotation equivariance constraints the filters and reduces their expressiveness, which hinders the learning process of the model. For general-purpose segmentation, like COCO-Stuff, equivariant U-Nets match the vanilla ones on performance metrics (see Table 7). For those general tasks, the performance gap arises in small data regimes, where equivariant models are consistently worse than the vanilla ones. This shows that low data availability affects the trade-off between architectural constraints and model expressiveness. In particular,  $D_4$  consistently shows lower performance across datasets, suggesting that stronger symmetry constraints may be too restrictive for practical segmentation tasks.

**Small models in large data settings** In terms of evaluation metrics, equivariant models can be preferable to their vanilla counterpart depending on the task. For example, it is the case for the Kvasir-SEG dataset and the URDE dataset, where results show that  $E(2)$ -U-Net can achieve better performances (only requiring slightly more computation time for Kvasir-SEG). However, as far as the NucleiSeg dataset is concerned, vanilla U-Nets seem to be a better choice than equivariant U-Nets, as they achieve better or at least top performances regarding all the different metrics. This can be explained by the fact that object of interest in NucleiSeg are all of circular shape. In such situation where the object of interest already satisfy the rotational symmetry by itself (rotation of the object of interest has no impact on the observed shape), applying constraints on the filters like in group-CNNs is meaningless, and even lead to an unnecessary reduction of the expressiveness of the filters, leading to lower levels of performance.

Regarding the COCO-Stuff and iSAID datasets, the vanilla U-Nets achieve better overall performances. However, for COCO-Stuff, the  $C_4$  equivariant U-Net is able to achieve similar performances, only requiring a larger training time. Regarding the iSAID dataset, equivariant models seems to struggle achieving the vanilla performances, which is even more true for the  $D_4$  equivariant model. This may be explained by the fact that the prior knowledge of rotation equivariance is not worth the reduction in expressiveness in the filter. Indeed, only rotation equivariant features can be extracted, which is a constraint that reduce the search space when optimizing the filters, and which is sometimes not beneficial. This insight can also be confirmed by looking at the  $D_4$  models that are always significantly below the other ones in terms of performance, and which further constraints the shape of the filters by including a reflection symmetry.

**Large models in large data settings** Regarding the first three datasets, i.e., Kvasir-SEG, NucleiSeg and URDE, conclusions are really similar to the previous ones using small models. However, one can point out that large models are always significantly better than their lightweight versions. Now, the results for the COCO-Stuff and iSAID datasets are more interesting. Indeed, for the first one, performances are significantly better, and the  $C_4$  and  $C_8$  models are now even better than the vanilla models according to mean IoU and mean accuracy. For the iSAID dataset, vanilla U-Net are still the best performing one and large differences still exist with their equivariant counterparts.

**Small models in small data settings** The results for this experimental setup are really similar to those already discussed. However, one can point out that the gap in performances is sometimes bigger. It means that significantly reducing the amount of data seems to exacerbate the advantage and disadvantage of the different methods.

**Large models in small data settings** Again, insights are similar to those already provided for the other settings. Using larger models seems beneficial as it significantly increases the overall performances. The URDE dataset is the only case where, for the vanilla U-Net, using a larger model lead to a small loss in performances. The observation of Figure 9 shows that the larger model under small data quickly stagnates at around 55% of IoU, with large up and down peaks in the metric between  $5 \times 10^2$  and  $3 \times 10^3$  seconds. The behaviour of the smaller model under the small data setting does not share this characteristic, and IoU remains at around 59% from  $5 \times 10^2$  seconds until the end of training.

**Final thoughts** Based on the results from Kvasir-SEG and NucleiSeg, one may conclude with a first insight that **equivariant U-Nets are an interesting choice to achieve better performances in tasks for which local rotations in the image have an impact on the final image, but does not contain any information**. It is the case for Kvasir-SEG, as polyps can be of arbitrary shape. However, the particular orientation of polyps in the image should not affect their segmentation. This last point is also true for NucleiSeg, but in this case **as nuclei are not of arbitrary shape but are instead always of circular shape, using rotation equivariance is detrimental to the performance**. One additional factor of explanation lies with the vast quantity of objects that are present in each image, making the task more difficult for equivariant U-Nets.

Regarding datasets that focus on more general tasks, such as COCO-Stuff, equivariant models can achieve similar performances than their vanilla counterparts. However, **if equivariant features are used alone (without introducing non-equivariant features in the model), results show that it is preferable to consider sufficiently large models**. Indeed, the loss in expressiveness in the filters makes it difficult for the small models to capture enough features in the images. Nonetheless, the fact that equivariant U-Nets are able to achieve similar performances when increasing the number of filters indicate that they are able to extract meaningful features. Thus, for tasks that are more general and involve complex object segmentations, **one could benefit from new models that are specifically designed to extract both equivariant and non-equivariant features in parallel**.

## 6.2 Discussion in terms of computational resources

Achieving the best performances in terms of evaluation metrics is of course of primary importance for many tasks. However, it is also important to consider the amount of computational resources (and time) that are involved in the training process of the models. For example, for some applications, it could be interesting to consider a particular model even if it leads to slightly smaller performances if it could save a significant amount of time. For this purpose,  $E(2)$ -U-Net are an interesting candidate. This second part of the discussion will more focus on the question of sustainability. In other words: “is it possible to obtain a good trade-off between performances and training time?”

For many of the experimental setups that were considered,  $E(2)$ -U-Nets are able to achieve better or similar performances. However, we only observe for a few particular cases (URDE, small and large models on large data settings, and iSAID, small models and small data settings) potential gains in terms of computational resources. In other cases, the IoU with respect to the training time are similar or convergence is slightly slower for equivariant models. This can be explained by the fact that even if rotation equivariance is meaningful, using group-convolutions is more expensive than vanilla convolutions. The analysis of the results reveals that adding more computational resources does not always justify the marginal improvements in epoch-wise convergence. This finding challenges the assumption that equivariant models are universally beneficial for reducing training time while the optimal choice depends heavily on the specific task requirements. The experiments consistently show that both larger models and larger data regimes correlate with higher performance. Nonetheless, **the relationship between these factors reveals an important asymmetry: reducing the training dataset size has a substantially more detrimental effect on model performance compared to reducing model size, despite both approaches decreasing training time**. If one wants to obtain a good trade-off between performance and training time, using smaller models appears a better approach over using smaller training dataset size.

## 7 Conclusion and limitations

In this work, the performance of vanilla and equivariant U-Nets is assessed across five diverse datasets, namely Kvasir-SEG, NucleiSeg, URDE, COCO-Stuff, and iSAID. They vary in size, have or do not have rotation-invariant characteristics, and focus on specific, narrow tasks or on tasks that are more general. This enables the examination of the effects of model size, dataset characteristics, and segmentation task type (i.e., binary or semantic segmentation). The intention behind such analysis is to get a better understanding of how architectural constraints, such as rotation equivariance, impact the performance and computational efficiency of segmentation models.

The findings of this study highlight that equivariant U-Nets (and more specifically, rotation equivariant models), particularly  $E(2)$ -U-Nets based on the use of discrete symmetry groups like  $C_4$ ,  $C_8$  or  $D_4$ , provide advantages in datasets with high orientation variability, such as Kvasir-SEG and URDE, where equivariant models outperformed their vanilla counterparts. However, in datasets like NucleiSeg, where the objects exhibit inherent rotational symmetry, vanilla U-Nets achieved higher accuracy and expressiveness. For larger, more complex datasets such as COCO-Stuff and iSAID, vanilla U-Nets consistently demonstrated superior performance. This shows that equivariance constraints may not always translate to improved performance, especially in settings requiring broader feature expressiveness. Moreover, we find that reducing the number of training data (i.e., small data setting with only 10% of each training fold data) does not have a significant impact on the relative performance.

An important future work will be to design and test models that are able to build a set of both equivariant and non-equivariant features. Our experiments highlight the fact that for more complex datasets like COCO-Stuff or iSAID, equivariance is less useful. Still, they are able to extract useful features and can achieve almost state-of-the-art performances. Thus, we believe that those equivariant features can extract complementary information that could benefit to the model.

## References

- Holger Caesar, Jasper Uijlings, and Vittorio Ferrari. Region-based semantic segmentation with end-to-end training. In *Computer Vision – ECCV 2016*, pp. 381–397, 2016.
- Holger Caesar, Jasper Uijlings, and Vittorio Ferrari. Coco-stuff: Thing and stuff classes in context. In *2018 IEEE/CVF Conference on Computer Vision and Pattern Recognition (CVPR)*, pp. 1209–1218. IEEE Computer Society, 2018.
- Benjamin Chidester, That-Vinh Ton, Minh-Triet Tran, Jian Ma, and Minh N. Do. Enhanced rotation-equivariant u-net for nuclear segmentation. In *2019 IEEE/CVF Conference on Computer Vision and Pattern Recognition Workshops (CVPRW)*, pp. 1097–1104, 2019a.
- Benjamin Chidester, Tianming Zhou, Minh N Do, and Jian Ma. Rotation equivariant and invariant neural networks for microscopy image analysis. *Bioinformatics*, 35(14):i530–i537, 2019b.
- Taco S Cohen and Max Welling. Group equivariant convolutional networks. In *International Conference on Machine Learning (ICML)*, pp. 2990–2999, 2016.
- Taco S Cohen and Max Welling. Steerable CNNs. In *International Conference on Learning Representations (ICLR)*, 2017.
- Asanka De Silva, Rajitha Ranasinghe, Arooran Sounthararajah, et al. A benchmark dataset for binary segmentation and quantification of dust emissions from unsealed roads. *Sci. Data*, 10(1):14, 2023.
- Valentin Delchevalerie, Alexandre Mayer, Adrien Bibal, and Benoît Frénay.  $SO(2)$  and  $O(2)$  Equivariance in Image Recognition with Bessel-Convolutional Neural Networks. *arXiv:2304.09214*, 2023.
- David Eigen and Rob Fergus. Predicting depth, surface normals and semantic labels with a common multi-scale convolutional architecture. In *2015 IEEE International Conference on Computer Vision (ICCV)*, pp. 2650–2658, 2015.

- Axel Elaldi, Guido Gerig, and Neel Dey.  $E(3) \times so(3)$ -equivariant networks for spherical deconvolution in diffusion mri. In *Medical Imaging with Deep Learning*, volume 227 of *Proceedings of Machine Learning Research*, pp. 301–319. PMLR, 2024.
- Simon Graham, David Epstein, and Nasir Rajpoot. Dense steerable filter CNNs for exploiting rotational symmetry in histology images. *IEEE Transactions on Medical Imaging*, 39(12):4124–4136, 2020.
- Andrew Janowczyk and Anant Madabhushi. Deep learning for digital pathology image analysis: A comprehensive tutorial with selected use cases. *Journal of Pathology Informatics*, 7(1):29, 2016.
- Debesh Jha, Pia H. Smedsrud, Michael A. Riegler, et al. Kvasir-seg: A segmented polyp dataset. In *MMM*, pp. 451–462, 2020.
- Abhay Kumar, Nishant Jain, Chirag Singh, and Suraj Tripathi. Exploiting sift descriptor for rotation invariant convolutional neural network. In *IEEE India Council International Conference (INDICON)*, pp. 1–5, 2018.
- Linhao Li, Zhiqiang Zhou, Bo Wang, Lingjuan Miao, and Hua Zong. A novel CNN-based method for accurate ship detection in HR optical remote sensing images via rotated bounding box. *IEEE Transactions on Geoscience and Remote Sensing*, 59(1):686–699, 2020.
- Tsung-Yi Lin, Michael Maire, Serge J. Belongie, Lubomir D. Bourdev, Ross B. Girshick, James Hays, Pietro Perona, Deva Ramanan, Piotr Dollár, and C. Lawrence Zitnick. Microsoft COCO: common objects in context. *CoRR*, abs/1405.0312, 2014.
- Jonathan Long, Evan Shelhamer, and Trevor Darrell. Fully convolutional networks for semantic segmentation. In *2015 IEEE Conference on Computer Vision and Pattern Recognition (CVPR)*, pp. 3431–3440, 2015.
- Ilya Loshchilov and Frank Hutter. Decoupled weight decay regularization. In *International Conference on Learning Representations*, 2019.
- Diego Marcos, Michele Volpi, and Devis Tuia. Learning rotation invariant convolutional filters for texture classification. In *International Conference on Pattern Recognition (ICPR)*, pp. 2012–2017, 2016.
- Diego Marcos, Michele Volpi, Benjamin Kellenberger, and Devis Tuia. Land cover mapping at very high resolution with rotation equivariant cnns: Towards small yet accurate models. *ISPRS Journal of Photogrammetry and Remote Sensing*, 145:96–107, 2018.
- Joshua Mitton and Roderick Murray-Smith. Rotation equivariant deforestation segmentation and driver classification. *NeurIPS 2021 Workshop on Tackling Climate Change with Machine Learning*, 2021.
- Vinod Nair and Geoffrey E. Hinton. Rectified linear units improve restricted boltzmann machines. In *Proceedings of the 27th International Conference on International Conference on Machine Learning, ICML’10*, pp. 807–814, 2010.
- Valentin Oreiller, Julien Fageot, Vincent Andrearczyk, John O. Prior, and Adrien Depeursinge. Robust multi-organ nucleus segmentation using a locally rotation invariant bispectral u-net. In *Proceedings of The 5th International Conference on Medical Imaging with Deep Learning*, volume 172 of *Proceedings of Machine Learning Research*, pp. 929–943. PMLR, 2022.
- Facundo Quiroga, Franco Ronchetti, Laura Lanzarini, and Aurelio F Bariviera. Revisiting data augmentation for rotational invariance in convolutional neural networks. In *International Conference on Modelling and Simulation in Management Sciences*, pp. 127–141, 2018.
- Joseph Redmon, Santosh Divvala, Ross Girshick, and Ali Farhadi. You Only Look Once: Unified, Real-Time Object Detection. In *2016 IEEE Conference on Computer Vision and Pattern Recognition (CVPR)*, pp. 779–788, 2016.

- O. Ronneberger, P. Fischer, and T. Brox. U-net: Convolutional networks for biomedical image segmentation. In *Medical Image Computing and Computer-Assisted Intervention (MICCAI)*, volume 9351 of *LNCS*, pp. 234–241, 2015.
- Carole H. Sudre, Wenqi Li, Tom Vercauteren, Sebastien Ourselin, and M. Jorge Cardoso. Generalised dice overlap as a deep learning loss function for highly unbalanced segmentations. In *Deep Learning in Medical Image Analysis and Multimodal Learning for Clinical Decision Support*, pp. 240–248, Cham, 2017.
- Syed Waqas Zamir, Aditya Arora, Akshita Gupta, Salman Khan, Guolei Sun, Fahad Shahbaz Khan, Fan Zhu, Ling Shao, Gui-Song Xia, and Xiang Bai. isaid: A large-scale dataset for instance segmentation in aerial images. In *Proceedings of the IEEE/CVF Conference on Computer Vision and Pattern Recognition (CVPR) Workshops*, June 2019.
- Maurice Weiler and Gabriele Cesa. General  $E(2)$ -Equivariant Steerable CNNs. In *Advances in Neural Information Processing Systems (NeurIPS)*, 2019.
- Maurice Weiler, Fred A Hamprecht, and Martin Storath. Learning steerable filters for rotation equivariant CNNs. In *IEEE Conference on Computer Vision and Pattern Recognition (CVPR)*, pp. 849–858, 2018.
- Daniel E Worrall, Stephan J Garbin, Daniyar Turmukhambetov, and Gabriel J Brostow. Harmonic networks: Deep translation and rotation equivariance. In *Proceedings of the IEEE Conference on Computer Vision and Pattern Recognition (CVPR)*, pp. 5028–5037, 2017.
- Gui-Song Xia, Xiang Bai, Jian Ding, Zhen Zhu, Serge Belongie, Jiebo Luo, Mihai Datcu, Marcello Pelillo, and Liangpei Zhang. Dota: A large-scale dataset for object detection in aerial images. In *2018 IEEE/CVF Conference on Computer Vision and Pattern Recognition (CVPR)*, pp. 3974–3983, 2018.